559 **Figure captions**

560 Fig. 1 Spatial location and characteristics of the HRB.

561 Fig. 2 Annual runoff at different hydrological stations and water diversion in the
562 upstream of the agricultural area in HRB.

563 Fig. 3 Distribution of trend slopes per decade of E_{pen}, E_{rad}, and E_{aero} in the different
564 stations in the HRB (1970–2017).

565 Fig. 4 Annual variations of the averaged E_{pen}, E_{rad}, and E_{aero} in different regions in the
566 HRB.

567 Fig. 5 Relationship between the variations of potential and actual evaporation in the
568 HRB.

569 Fig. 6 Fitting of the E_{pen} variation calculated by the regression and trend analytical
570 methods in the HRB.

571

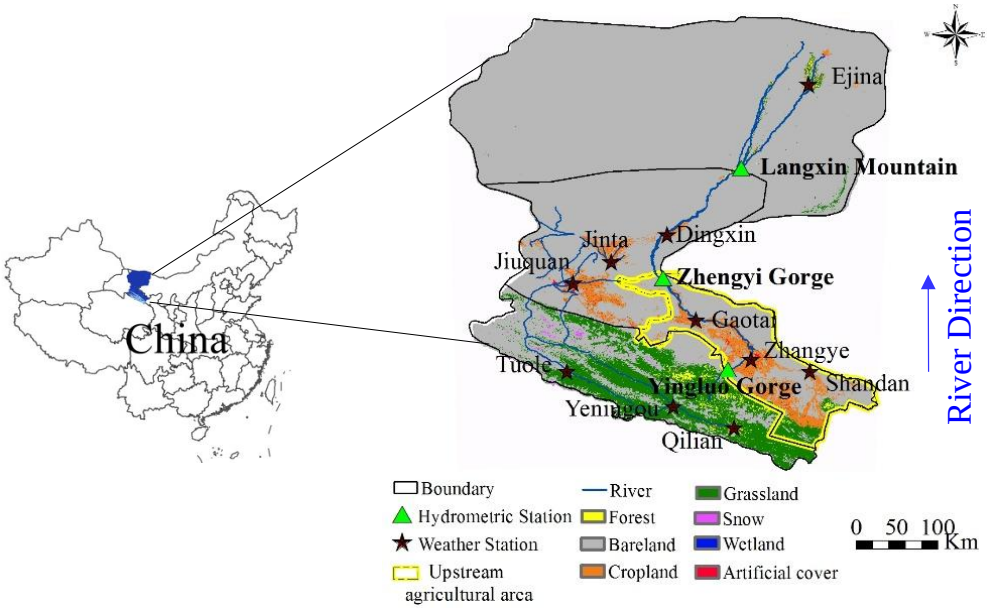

572 Fig. 1. Spatial location and characteristics of the HRB

573

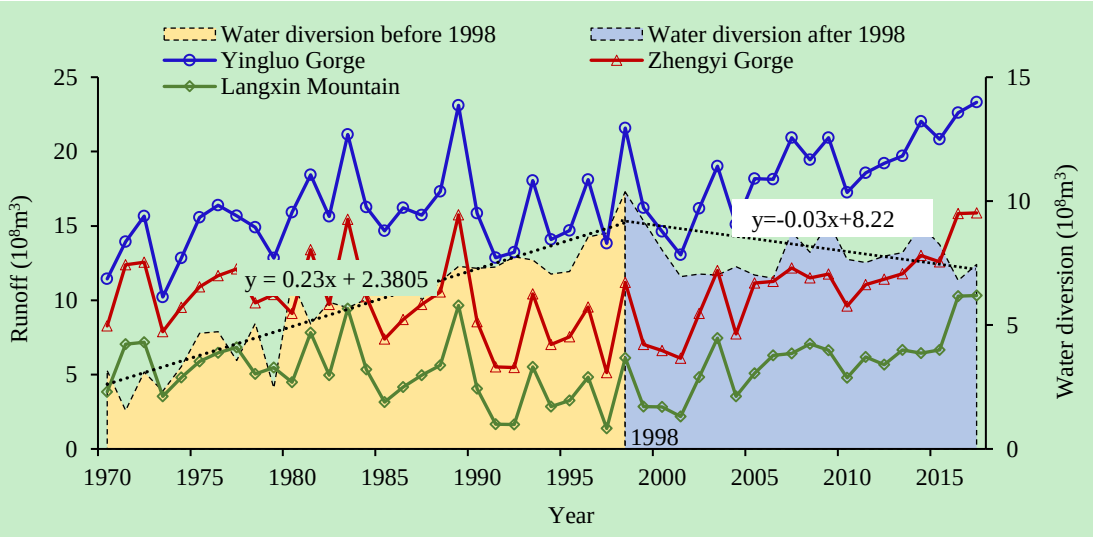

574 Fig. 2. Annual runoff at different hydrological stations and water diversion in the
575 upstream of the agricultural area in HRB

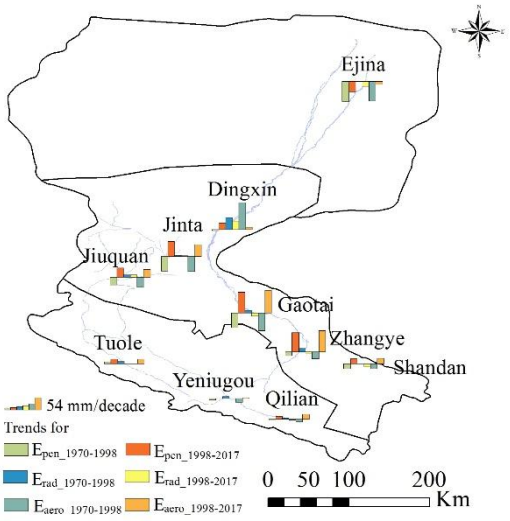

576

577 Fig. 3. Distribution of trend slopes per decade of E_{pen}, E_{rad}, and E_{aero} in the different

578 stations in the HRB (1970–2017)

579

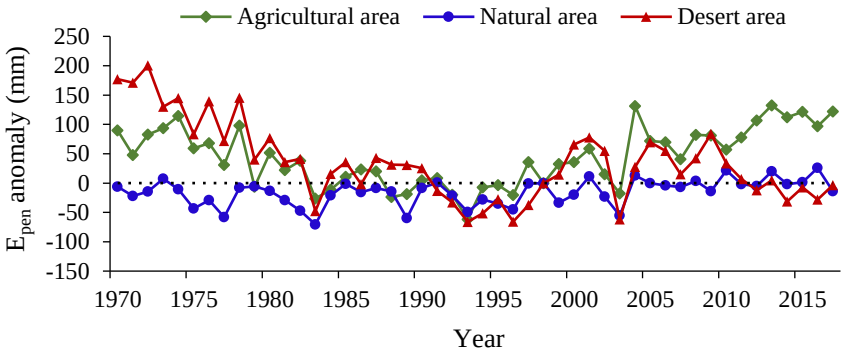

(a)

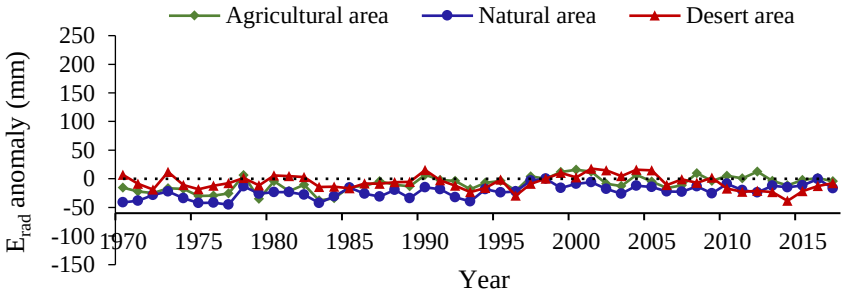

(b)

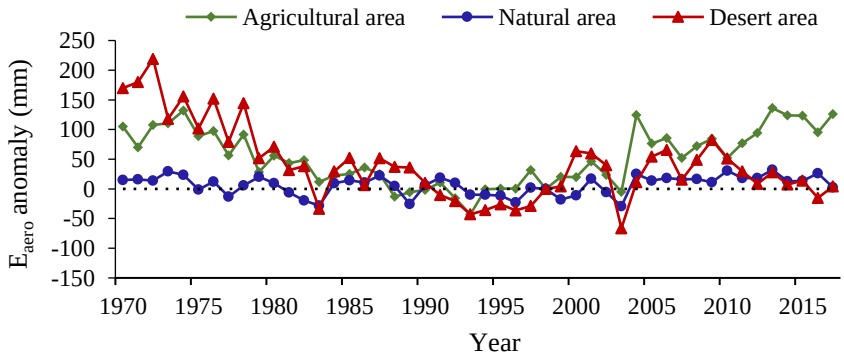

(c)

580 Fig. 4. Annual variations of the averaged E_{pen}, E_{rad}, and E_{aero} in different regions in the

581 HRB

582

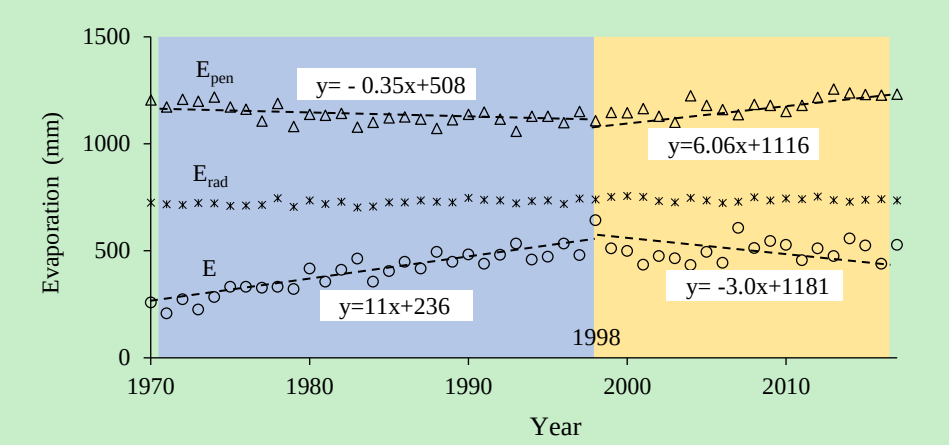

583 Fig. 5. Relationship between the variations of potential and actual evaporation in the

584 HRB

585

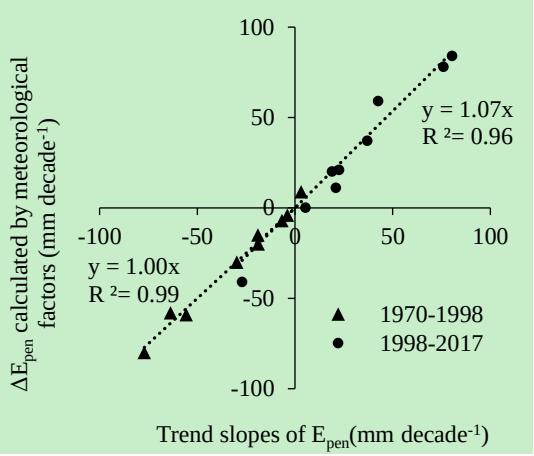

586 Fig. 6. Fitting of the E_{pen} variation calculated by the regression and trend analytical

587 methods in the HRB

588